J. Iran. Chem. Soc., Vol. 6, No. 3, September 2009, pp. 489-503.

JOURNAL OF THE
Iranian
Chemical Society

Evolution of the H_2^+ Electron Wavepacket under Magnetic and Electric Fields of Ultrashort Intense Laser Pulse

H. Ebadi and H. Sabzyan*
Department of Chemistry, University of Isfahan, Isfahan 81746-73441, I. R. Iran

(Received 29 May 2008, Accepted 5 July 2008)

Magnetic interaction was included in the simulation of the evolution of the electron wave-packet of the hydrogen molecular ion H_2^+ in femtosecond intense pulsed laser fields applied along the molecular axis. This evolution was followed by solving 2-D time-dependent Schrödinger equation at some fixed inter-nuclear separations. Magnetic interaction effects at non-relativistic intensities induced a phase shift in the time evolution of the electron wave-packet, and an excess z-component angular momentum as compared with the results obtained in the absence of magnetic interaction. Furthermore, the H_2^+ electron WP displacement showed a drift and wiggling in the propagation direction which was different from that observed under pure electric field of the laser pulse. The local fluxes at different points of the 2-D space borders and the time-dependent induced angular momentum are calculated and analyzed.

Keywords: Intense laser field, TDSE, H_2^+, Wavepacket, Magnetic interaction, Angular momentum, Ionization rate

INTRODUCTION

In the past two decades, a number of interesting phenomena related to the interaction of atoms and molecules with ultra-short laser pulses have been observed and studied theoretically and experimentally [1-3]. Over the past decade, powerful computational hardware and software facilities have allowed numerical solution of the 1-D and 2-D (ρ,z) time-dependent Schrödinger equation (TDSE), and attempts towards the solution of the full dimensional H_2^+, including electronic and nuclear dynamics, have been in order in this field of physics [4-6]. Results of these studies effectively describe phenomena of the electric interaction of short pulse lasers with atoms and molecules [7-9].

The classical electron trajectories in the continuum states and evolution of the quantum mechanical electron wave-packet (WP) have been used to gain better insights into the physics of these phenomena [10,11]. Most of the theoretical studies in this field of science are based on the dipole approximation for laser-atom/molecule interactions [2-5]. In this approximation, which is used widely in theoretical studies of strong-field phenomena, spatial dependence of the vector potential of the electromagnetic field is ignored. Similarly, in most reported works, magnetic field effects on the response of the atomic and molecular species to strong laser fields are also neglected [7-9,12]. Most of the previous studies include only the interaction of the electric field of the intense laser pulse with matter. Such approximation is valid for the laser intensities not high enough to accelerate the electrons to relativistic velocities. Relativistic mass change is at least second order in v/c, whereas the drift due to the magnetic field is first order in v/c, and therefore, the magnetic field effect, appearing first as the increase in the field strength, drives the electron to higher velocities [11,12]. There are some classical relativistic analyses [13,14] and quantum mechanical studies [10,11,15] on the influence of the magnetic field of intense

*Corresponding author. E-mail: sabzyan@sci.ui.ac.ir

laser fields on the atomic electron dynamics. However, there exist only a few reports on the theoretical study of the magnetic field effect on the molecular electron dynamics and electron WP evolution via solving the TDSE [16].

Electron dynamics (classical electron trajectories and quantum mechanical WP evolution) is sensitive to the factors such as the magnetic field which leads to the trajectory or WP distortions. For example, production of high harmonic generation (HHG) is very sensitive to the recollision process of the electron WP to the parent ion [16]. An important factor which is crucial for the HHG is the magnetic field of the laser pulse [1,11]. The reason is that the Lorentz force exerted by the magnetic field component of the laser pulse deflects electron trajectory or WP along the propagation direction and diminishes the electron interaction with the parent ion. Magnetic field interaction determines also the recollision of the ionized (free) electron with the parent molecule, which has an important role in the pattern of fragmentation and its consequent ionization steps [17,18]. The deflection of the WP by the magnetic field of the laser pulse can be significant for attosecond pulses in the few-optical-cycle regime, since electrons detached from the parent atom or molecule during the fast turn-on of the intense laser pulse can be accelerated to very high velocities back towards the parent ion [19]. Electron velocities just sufficient for the Lorentz force-induced suppression of the attosecond pulses with intensities below 10^{17} Wcm^{-2} are significantly smaller than the speed of light, and thus non-relativistic quantum mechanics remains valid in this case.

The magnetic field component of the laser pulse due to Lorentz force results in a drift of the electron WP in the propagation direction, the extent of drift and the trajectory of the WP is strongly related to the intensity and the frequency of the incident light. This, consequently, has distinct effects on the photon emission and the angle resolved ionization of the molecular system in the polarization direction.

In this work, we studied the coupling of the magnetic field of the intense laser pulse with orbital angular momentum of electron and its effects on the dynamics of of the electron WP evolution and its consequent ionization rate of a 2-D model of H_2^+ molecular ion. The ionization behavior of the hydrogen molecular ion at the equilibrium inter-nuclear distance was different from that at the critical inter-nuclear distance (around 6-7 au) and higher inter-nuclear distances (higher than 10 au). We studied the magnetic field effect of the laser pulse on the ionization dynamics at a set of important inter-nuclear distances. Simulation of the WP evolution was carried out with the long-wavelength Ti:sapphire laser with non-relativistic intensities falling in the tunneling regime. In order to visualize the magnetic field effect, we calculated and analyzed total and local fluxes in each direction of the simulation box in addition to the average value of the drift of the electron in the propagation direction. Our results show that even with a long-wavelength laser pulse, the magnetic field of the laser pulse breaks the symmetry of the angle-resolved ionization and the fluxes at the borders along the polarization direction. Details of this evolution were studied by following the induced angular momentum, and visualized in the animations made of a sequence of the instantaneous evolving WPs of the system.

COMPUTATIONAL MODEL

There is a range of values for the laser parameters (*ca*., laser intensities between 10^{14} and 10^{16} Wcm^{-2}) at which velocity of electron is small enough to work on the assumption that the electron dynamics is given by the Schrödinger equation, and large enough to include the first-order relativistic corrections. In this range, within the Born-Oppenheimer approximation, the TDSE for electronic wavefunction of the H_2^+ molecule with the combined scalar potential, $V(\vec{r}\,)$, and the external time-dependent magnetic and electric fields, $\vec{B}(\vec{r},t)$ and $\vec{E}(\vec{r},t)$, has the following form in atomic units ($e = 1$, $m_e = 1$, $\hbar = 1$, $c = 137$):

$$i\frac{\partial\Psi(\vec{r},t)}{\partial t} = \left[-\frac{1}{2}\nabla^2 + V(\vec{r}) + \vec{r}\cdot\vec{E}(\vec{r},t) + \frac{1}{2c}\vec{L}\cdot\vec{B}\right]\Psi(\vec{r},t) \qquad (1)$$

This Equation may be regarded as the expansion of the vector potential of the electromagnetic field to the first order beyond the dipole approximation in the velocity gauge in which we have assumed that $\vec{B}$ is spatially uniform. In Eq. (1), Hamiltonian has been improved to include the magnetic interaction term in its most simple way. A complete picture of the interaction process, of course, in the 3-D space, can only be obtained by the complete Hamiltonian in the velocity gauge not intended in this point of the study. For the 2-D H_2^+ molecule aligned in the x axis, the soft-core scalar Coulomb

potential in the *xy* plane is given by

$$V(x,y) = -\frac{1}{((x-R/2)^2+y^2+a)^{1/2}} - \frac{1}{((x+R/2)^2+y^2+a)^{1/2}} \qquad (2)$$

where R is the inter-nuclear distance and a is a parameter that allows avoiding singularities at the origins, and is chosen to be a = 0.52 in our calculations. The spatial adaptive (non-uniform) grid [7] used in these calculations has 570-620 points along the x coordinate and 545 points along the y coordinate.

The spatial borders of the simulation box, as shown in Fig. 1, are set (in atomic unit) at (-90 and 90) and (-80 and 80) respectively in the x and y directions. In this grid, and for the chosen value of a, the ground state of the *xy* 2-D model of H_2^+ has an energy of E_g = -0.6, as determined by the standard imaginary-time propagation method. The excited states of the H_2^+ molecule are determined numerically using imaginary time Gram-Schmitt orthogonalization method. Polarization and the wave vector of the laser pulse are assumed to be along the x and y axes, respectively.

The reference frame of our system is depicted in Fig. 1. The spatial dependence of the field has been neglected and dipole approximation is assumed. Therefore, the monochromatic electric and magnetic fields applied to the H_2^+ molecular ion take the forms

$$E_x(t) = E_{0x} f(t)\cos(\omega t) \quad , \quad B_z(t) = B_{0z} f(t)\cos(\omega t) \qquad (3)$$

where E_{0x} and B_{0z} are the maximum strengths of the electric and magnetic fields of the laser pulse, and ω is its angular frequency.

In Eq. (3), $f(t)$ is an envelope function with a ramp-on from 0 to 1 during the time t_1, then constant, 1, from t_1 to $t_1 + t_2$ and with a ramp-off to 0 during $t_1 + t_2$ to $t_1 + t_2 + t_3$; a pulse scheme of (t_1 , t_2 , t_3) with the overall duration of $t_1 + t_2 + t_3$. We have used the following form for the envelope of the laser field:

$$f(t) = \begin{cases} \frac{1}{2}\left(1-\cos\left(\frac{\pi t}{t_1}\right)\right) & 0 < t \le t_1 \\ 1 & t_1 < t \le t_1 + t_2 \\ \frac{1}{2}\left(1-\cos\left(\frac{\pi(t-(t_1+t_2+t_3))}{t_2}\right)\right) & t_1+t_2 < t \le t_1+t_2+t_3 \\ 0 & t_1+t_2+t_3 \le t \end{cases} \qquad (4)$$

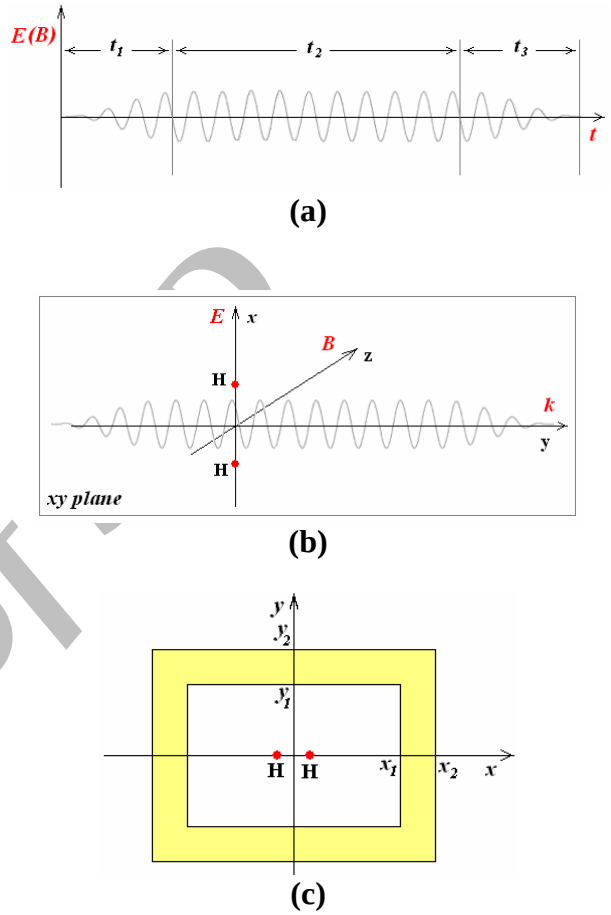

Fig. 1. The pulse scheme (a), the reference frame (b) and the simulation box setup (c) used in this work to study interaction of the H_2^+ system with intense laser pulse. The magnetic part of the laser pulse which lies in the yz plane is not shown to avoid complexity. Note that the pulse is not space-dependent and it is drawn in (b) only to depict direction of the passage of the pulse. The shaded part in (c) shows the region over which the NIP (Eq. (7)) is operative.

In our study, t_1, t_2 and t_3 are chosen to be 4, 10 and 4 cycles of the laser pulse, respectively. Therefore, we used a pulse scheme of (4,10,4) with the total duration of 18 cycles, as defined in Eq. (4). This pulse scheme is demonstrated in Fig. 1.

In order to avoid reflection of the WP at the boundaries, a negative imaginary potential (NIP), that absorbs the WP near

the boundaries, is added to the Hamiltonian [4]. For the *xy* 2-D system of our interest, in the presence of the combined magnetic and electric field of laser pulse, and with the Coulomb and NIP potentials, the TDSE becomes:

$$i\frac{\partial\Psi(x,y,t)}{\partial t}=\left[\begin{array}{l}-\frac{1}{2}\nabla^2_{x,y}+V(x,y)+\\ xE_x(t)+\frac{1}{2c}L_zB_z(t)+V_1(x,y)\end{array}\right]\Psi(x,y,t) \quad (5)$$

where $V(x,y)$ and $E_x(t)$ and $B_z(t)$ are given respectively by Eqs. (2) and (3), and the magnetic interaction term is given by

$$L_zB_z(t)=-i(x\frac{\partial}{\partial y}-y\frac{\partial}{\partial x})B_z(t)=-ix\frac{\partial}{\partial y}B_z(t)+iy\frac{\partial}{\partial x}B_z(t) \quad (6)$$

We have chosen the following form for the NIP $V_1(x,y)$ which is set on the borders of the grid box to act as an absorbing wall.

$$V_1(x,y)=\sum_{q=x,y}b_q\,V_1(q)\ ,\quad V_1(q)=-iV_{\circ q}\left[\frac{|q|-q_1}{q_2-q_1}\right]^{\alpha} \quad (7)$$

The *on-off* parameter b_q is set $b_q = 1$ in the $q_1 \le |q| \le q_2$ region and $b_q = 0$ elsewhere. Therefore, the values of q_1 and q_2 define the range in which the NIP is operative on the q coordinate. The adjustable parameters (α,β) and (V_{ox},V_{oy}), defining the NIP variations, are set respectively to $\alpha = \beta = 2.0$ and $V_{ox} = V_{oy} = 5.0$. In these calculations, borders of the effective region of the absorbing potential are set as ($x_1 = 70$, $x_2 = 90$) and ($y_1 = 60$ and $y_2 = 80$) for the x and y coordinates (Fig. 1). At the inner borders of the absorbing region ($|x| = x_1 = 70$ and $|y| = y_1 = 60$), the corresponding NIP is zero, and at the outer borders ($|x| = x_2 = 90$ and $|y| = y_2 = 80$) the NIP reaches its corresponding limiting values, V_{ox} and V_{oy}.

Equation (5) is solved numerically by a direct integration method using appropriate split operator scheme [9,20], as given below in Eq. (8), for the reduction of the numerical errors:

$$\begin{aligned}&\Psi(x,y,t+\Delta t)\cong\exp\left(-i\left(\hat{H}(x,y,t)\right)\Delta t\right)\Psi(x,y,t)\\ &=\exp\left(-i\left(\hat{H}_1(x,y,t)\right)\Delta t/2\right)\exp\left(-i\left(\hat{H}_2(x,y,t)\right)\Delta t\right)\\ &\exp\left(-i\left(\hat{H}_1(x,y,t)\right)\Delta t/2\right)\Psi(x,y,t)\end{aligned} \quad (8)$$

where $\hat{H}_1$ and $\hat{H}_2$ are chosen as

$$\hat{H}_1(x,y,t)=\left(-\frac{1}{2}\frac{\partial^2}{\partial x^2}+iy\frac{\partial}{2c\partial x}B_z(t)\right) \quad (9)$$

and

$$\hat{H}_2(x,y,t)=\left(-\frac{1}{2}\frac{\partial^2}{\partial y^2}+V(x,y)+xE_x(t)-ix\frac{\partial}{2c\partial y}B_z(t)+V_1(x,y)\right) \quad (10)$$

In order to study the contribution of the magnetic field of the laser pulse to the evolution of the electron WP of the H_2^+ molecular ion, Eq. (8) is solved for three different cases in which, in addition to the Coulomb and NIP potentials, Hamiltonian includes *i*) both magnetic and electric interaction terms; *ii*) only the electric interaction term (*i.e.* the last term in Eq. (9) and the fourth term in Eq. (10) are ignored), and *iii*) only the magnetic interaction term (*i.e.* the third term in Eq. (10) is ignored).

Each exponential term in Eq. (8) is evaluated using Crank-Nicholson finite-difference scheme [21]. Laser parameters used in our study are set first as $E_{x0} = 0.10676$ and $\omega = 0.0561$ which are equivalent to a laser pulse with $I = 4.0 \times 10^{14}$ Wcm^{-2} intensity and λ = 800 nm wavelength. The time step of calculations is set to $\Delta t = 0.02$ *au*. For this laser pulse, it was found that the pure magnetic field effect, *i.e.* contribution of the $B(t)$ containing terms in Eqs. (9) and (10), was very small. For the visualization of the pure magnetic field interaction effect on the evolution of the H_2^+ electron WP, intensity of the laser pulse was then set to $I = 4.0 \times 10^{18}$ W cm^{-2} in another set of simulations whose results are presented and discussed below. This intensity falls in the relativistic regime if the electric field is included in the Hamiltonian, and therefore a complete picture of the evolution at this intensity is pending upon a relativistic solution.

RESULTS AND DISCUSSION

The ionization rates corresponding to the evolution of the $|\Psi(t)|^2$ in the simulation box are calculated and plotted *vs.* R in Fig. 2 where they are compared with the corresponding results reported in literature [7,22-24]. This figure shows that R-dependence of the calculated ionization rates for our 2-D model (as well as those of the 1-D model [22]) are compatible with those obtained previously for the two-variable (ρ,z) 3-D

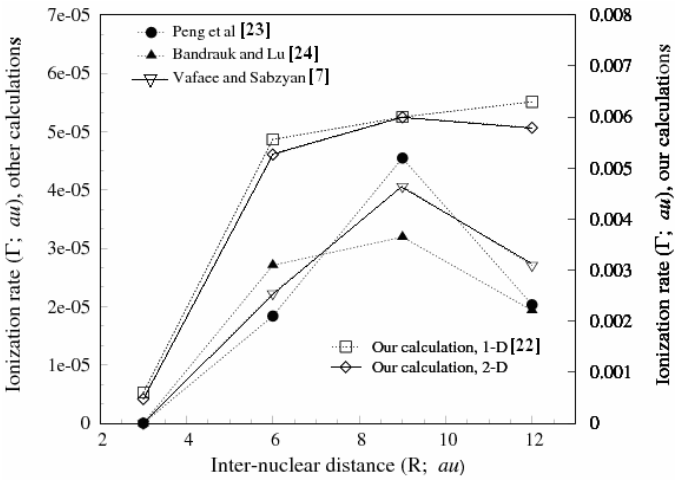

Fig. 2. Ionization rates calculated for the *xy* 2-D model of H_2^+ at different inter- nuclear separations in an intense laser pulse of $I = 4.0 \times 10^{14}$ W cm^{-2} intensity and $\lambda = 800$ nm wavelength, compared with the available data reported in our previous work [22] and in literature (for $I = 1.0 \times 10^{14}$ Wcm^{-2} and $\lambda = 790$ nm [7], $\lambda = 790$ nm [23], $\lambda = 800$ nm [24]). The right and left vertical scales are used to represent, respectively our (Ref. [22] and this work) and other (Refs. [7,23-24]) results.

systems [23-24]. However, as can be seen on the two corresponding vertical axes, the numerical values of the ionization rates obtained for the 1-D and 2-D models are larger by two orders of magnitude. This is quite natural as projection of the H_2^+ 3-D wavepacket onto the *xy* 2-D plane (or contraction of the wavepacket) results in higher kinetic energy which, in turn, results in higher ionization rates. The absolute value of the potential energy is also increased by this contraction, but application of the adjustment parameter *a*, in Eq. (2), set the potential back to its value for the 3-D system. It can thus be concluded that all numerical values of the ionization rates obtained for the 2-D model are considerably larger than the actual (experimental) ionization rates. Furthermore, the difference between the two sets of ionization rates in Fig. 2 at larger values of R can be attributed to different effects of the wavepacket contraction at different inter-nuclear separation. Application of a 2-D model in this work, although results in an overestimation of the ionization rates (whose exact evaluation has not been intended here), does not affect validity of the overall picture obtained for the contribution of the magnetic field to the evolution of the H_2^+ wavepacket in intense laser fields.

Variation of the electron probability density $|\Psi(t)|^2$ with time for the ground state of H_2^+ at R = 12.0 *au* is also calculated for the two different Hamiltonians (*i*) and (*ii*), and are demonstrated along with the differential norm $\Delta n = |\Psi(t)|^2_{(i)} - |\Psi(t)|^2_{(ii)}$ in Fig. 3. The pattern of the norm decay and the resulting ionization rates obtained for the *xy* 2-D model of H_2^+ (shown respectively in Figs. 2 and 1) are in qualitative agreement with the reported ionization rates for the 2-D (z, ρ) and 3-D models. Figure 3 shows that under the laser field, $|\Psi(t)|^2$ follows an exponential decay with a stepwise pattern caused by the oscillation of the laser field as found in the study of the 1-D model of H_2^+ [22]. These plateaus correspond to short periods of time just after the null points of the laser pulse electric field oscillations. Besides the significantly decreased ionization rate due to the decreased value of E prior to getting to the null point, it takes a finite time for the wavepacket to evolve from one boundary to the other when the sign of the electric field switches. Therefore, existence of the plateaus is a consequence of the sinusoidal oscillation of the electric field of the laser pulse. Since the ionization process is not immediate and needs a finite time to develop, plateaus of the norm curve appear with a time delay after the null points of the electric field. This time delay depends on the pulse envelop and the intensity of the laser field.

As can be seen from the time-behavior of the differential norm Δn in Fig. 3, magnetic field of the laser pulse shifts the phase of the norm decay which consequently results in a time delay in the ionization process. The corresponding time for this phase shift in the ionization process is about 7 *au* equivalent to 0.0625 cycle of the laser pulse with 4×10^{14} W cm^{-2} intensity and wavelength of 800 nm. This is a consequence of the magnetic interaction inducing changes in the trajectory of the electron wave-packet (WP) and ionization channel. Results of our calculations for the internuclear distance R = 3.0 *au* (not presented here for brevity), and their comparison with Fig. 3 show that the magnetic field effect on the variation of the WP norm and on the ionization rate is small and negligible when R is near the equilibrium inter-nuclear distance and the laser intensity is in the tunneling

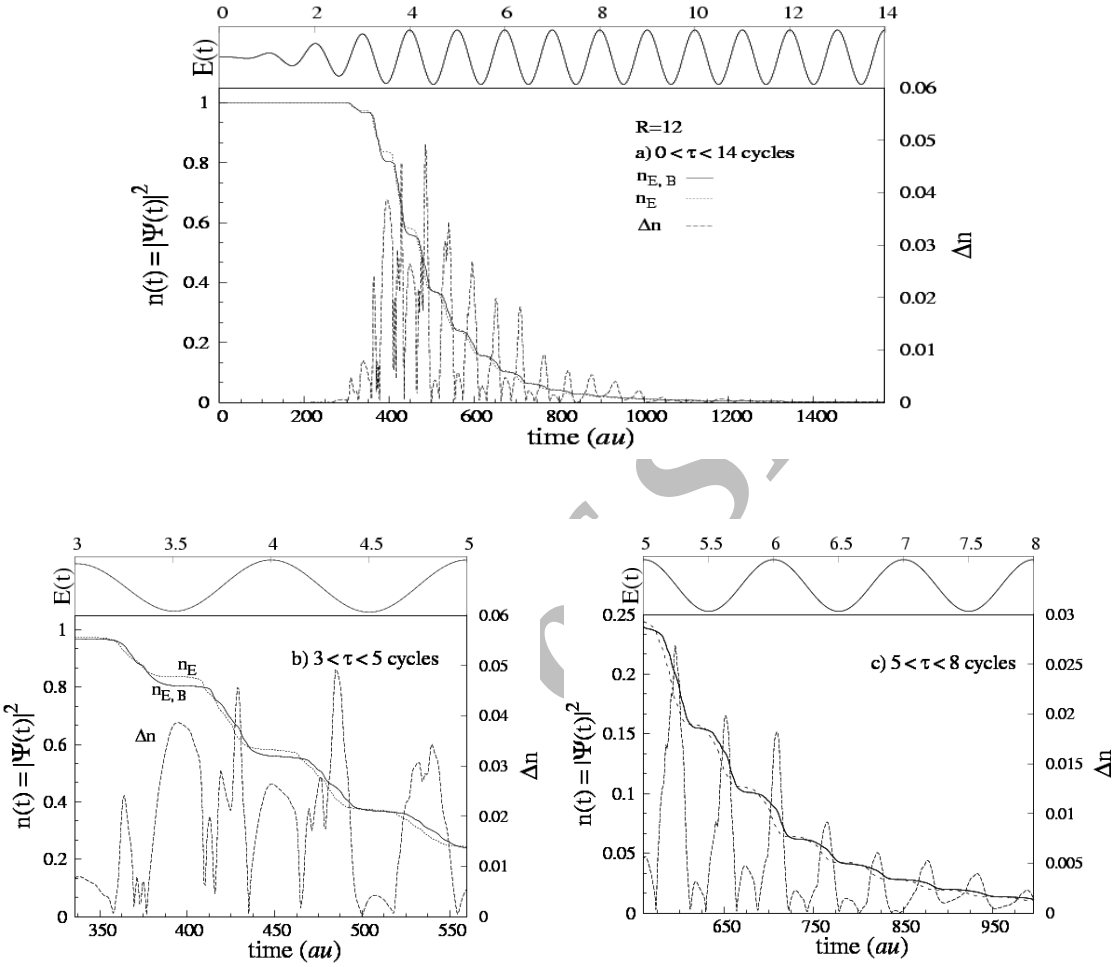

Fig. 3. Time evolution of the electron probability density (norm), $n(t) = |\Psi(t)|^2$, of the 2-D model of H_2^+ at inter-nuclear distance R = 12.0 *au* obtained under the influence of a (4,10,4) cycles laser pulse of I = 4.0×10^{14} Wcm^{-2} intensity and λ = 800 nm wavelength with the pulse shape given in Eq. (4) for the two Hamiltonian cases including (*i*) both the electric and magnetic field interactions ($n_{E,B}$), and (*ii*) the electric field interaction only (n_E). The differential norm, $\Delta n = n_{E,B} - n_E$, repre senting the contribution of the magnetic field of the laser pulse is also calculated and demonstrated. For better demonstration of the details of the time-dependent behavior of the norm, the curves are expanded in (b) and (c), respectively for time periods $3 < t < 5$ and $5 < t < 8$ cycles of the laser pulse, as shown atop of the diagrams.

regime. Typical values of the differential norm Δn for R = 3.0 *au* is on the order of 1×10^{-5} which is smaller by a factor of ~1000 as compared with those for R = 12.0 *au*. The local slope of the major WP components and their distribution in the simulation box are the two factors determining the weight of the magnetic interaction effect on the evolution of the WP. These factors are different at different inter-nuclear distances.

Flux of the electron probability density (at the boundaries of the grid box) is a useful quantity for characterization and better visualization of the electron wavepacket evolution. Analysis of the electron in- and out-fluxes, corresponding respectively to the negative and positive ionization rates [25],

can also be used for instantaneous probing of the details of the laser pulse magnetic field effects on this evolution. The electron probability flux is obtained as:

$$\vec{j}(\vec{r},t) = \mathrm{Im}(\Psi(\vec{r},t) * \nabla\Psi(\vec{r},t)) \qquad (11)$$

where $\vec{j}(\vec{r},t)$ is the instantaneous electron probability flux vector at the point $\vec{r}$ on the boundary, and $\Psi(\vec{r},t)$ is the time-dependent wavefunction. The overall flux of each boundary is obtained by summing up the local fluxes at all points of that boundary.

The overall fluxes of the time-dependent electron WP for different Hamiltonians (*i*) and (*ii*), in the two, polarization and propagation, directions (*x* and *y*, respectively) of the laser pulse at R = 12.0 *au* are calculated and demonstrated in Fig. 4. In this figure, the phase shift of the norm decay induced by the magnetic field interaction on the fluxes from each direction is evident.

As demonstrated and discussed above, for R = 12.0 *au* and at the laser intensity of 4.0×10^{14} Wcm^{-2}, contribution of the magnetic field effect to the ionization rate of the H_2^+ molecule is small (up to a maximum of 7%) as compared with that of

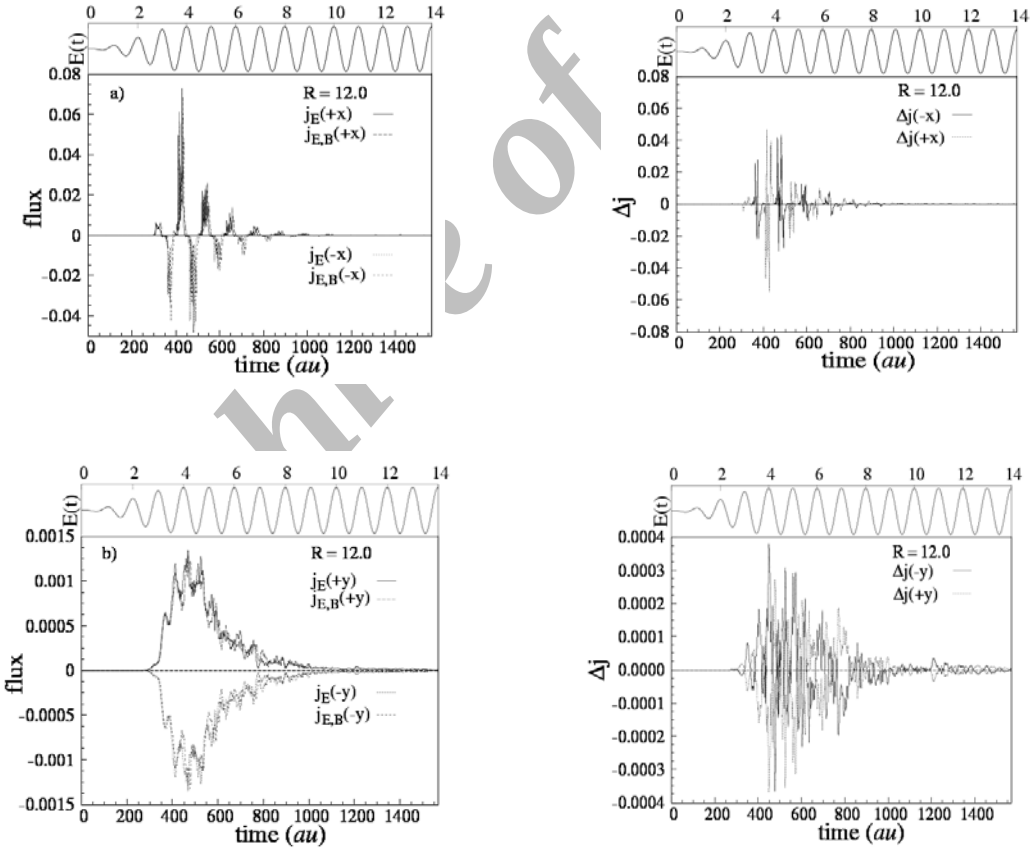

Fig. 4. Variation of the directional fluxes of the electron WP of the *xy* 2-D model of H_2^+ at inter-nuclear distance R = 12.0 *au* with time obtained under the influence of a (4,10,4) cycles laser pulse of $I = 4.0 \times 10^{14}$ Wcm^{-2} intensity and $\lambda = 800$ nm wavelength with and without the magnetic field interaction, $j_{E,B}$ and j_E, respectively, a) in the polarization (*x*), and b) in the propagation (*y*) direction of the laser pulse. The two plots on the right side demonstrate time-dependences of the corresponding differential fluxes, $\Delta j = j_{E,B} - j_E$. The corresponding pulse scheme is shown atop of all diagrams.

the pure electric field contribution, but has distinct effect on the trajectory of the electron WP which may result in changes in the ionization spatial pattern.

In the model used in our study, space angular momentum can have only the *z*-component (which is initially zero) and is generated during the course of evolution of the WP. This generated angular momentum interacts with the magnetic field of the laser pulse, which induces consequently noticeable excess angular momentum compared with the case in which the magnetic field effect is absent. The time dependent *z*-component angular momentum of the *xy* 2-D model of H_2^+ at some inter-nuclear distances (R = 3.0, 6.0, 9.0 and 12.0 *au*) calculated with and without magnetic interaction is shown in Fig. 5. This figure shows that at each inter-nuclear separation,

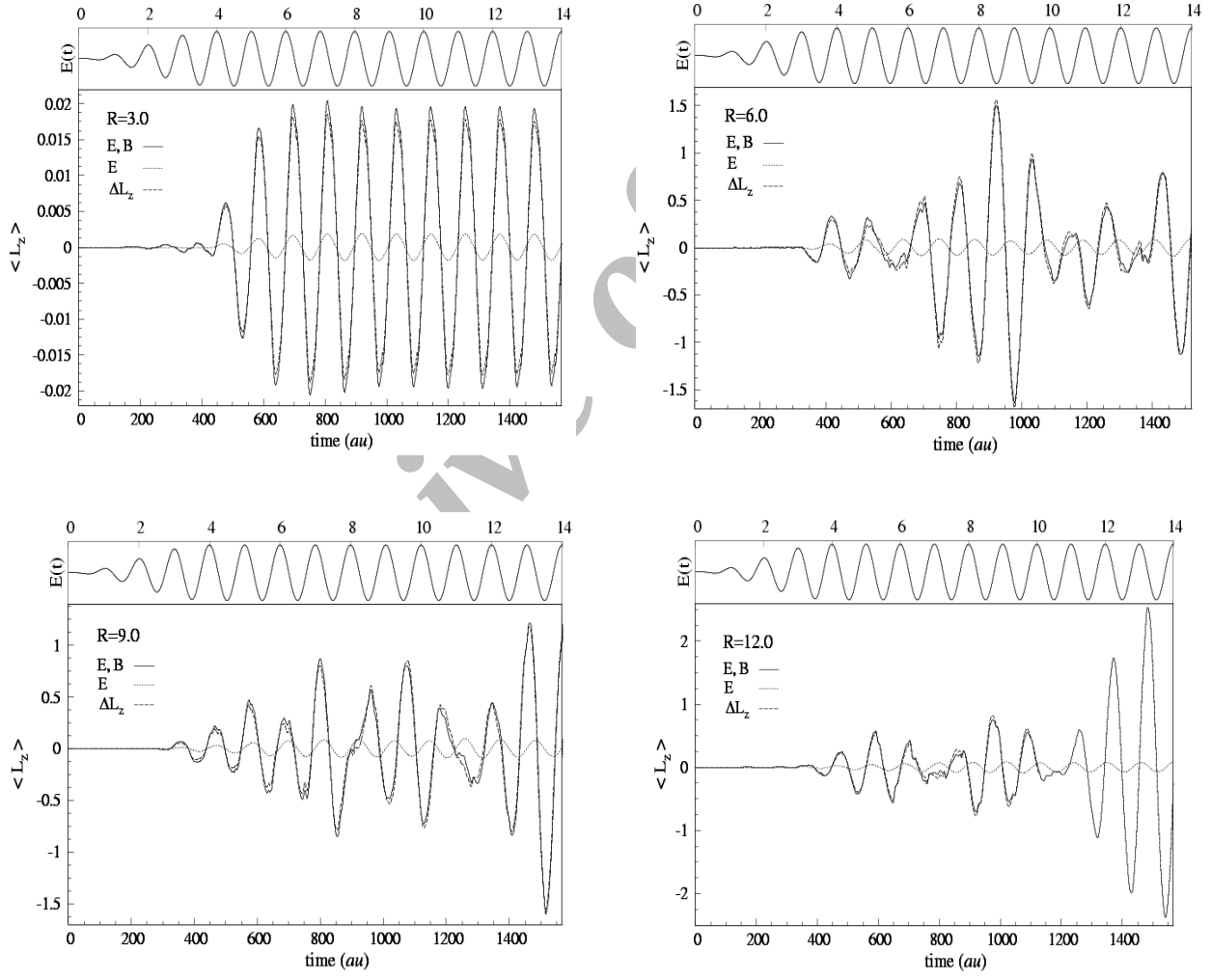

Fig. 5. Variation of the induced z-component angular momentum of the electron WP of the *xy* 2-D model of H_2^+ at inter-nuclear distances R = 3.0, 6.0, 9.0 and 12.0 *au* with time obtained under the influence of a (4,10,4) cycles laser pulse of $I = 4.0 \times 10^{14}$ Wcm^{-2} intensity and $\lambda = 800$ nm wavelength with and without the magnetic interaction, (E,B) and (E), respectively. The differential induced angular momentum, $\Delta L_z = < L_z >_{E,B} - < L_z >_E$, is also plotted to demonstrate contribution of the magnetic interaction. Note the different scales used for different parts. The corresponding pulse scheme is shown atop of all diagrams.

presence of the magnetic interaction (case (*i*)) induces more angular momentum as compared with the case when magnetic interaction is ignored (case (*ii*)). The maximum amplitude of the induced angular momentum in the presence of the magnetic interaction is larger by a factor of 10 compared to that in the absence of the magnetic field. At each inter-nuclear distance, the periodic pattern of the induced angular momentum in the absence of magnetic field is more regular. When R is near the equilibrium inter-nuclear distance, during the evolution, the WP is more compact and the induced angular momentum is small and has regular periodic pattern with the oscillation of the laser field even in the presence of the magnetic interaction. At the longer inter-nuclear distances, the spread of the WP by electric field of the laser pulse is more intensive and thus in the presence of the magnetic interaction, the induced excess angular momentum has non-regular periodic pattern.

The simple geometry of the evolved WP at small R, say 3.0 *au*, produces a simple temporal pattern for the induced angular momentum. Whereas the complex geometry of the evolved WP at critical and large R produces sectional angular momentum with different time phases whose resultant appears as a complex periodic time behavior pattern.

A useful observation showing explicitly the magnetic field effect on the evolution of the electron WP was the time-dependent perpendicular displacement (in the propagation direction of the laser field). The time-dependent average value of the electron WP displacement in the propagation direction, $\langle y(t) \rangle$, was calculated for different values of R and plotted in Fig. 6. In this figure, results of the same calculations carried out for hydrogen atom are also shown for comparison. These calculations were carried out for laser fields of the same

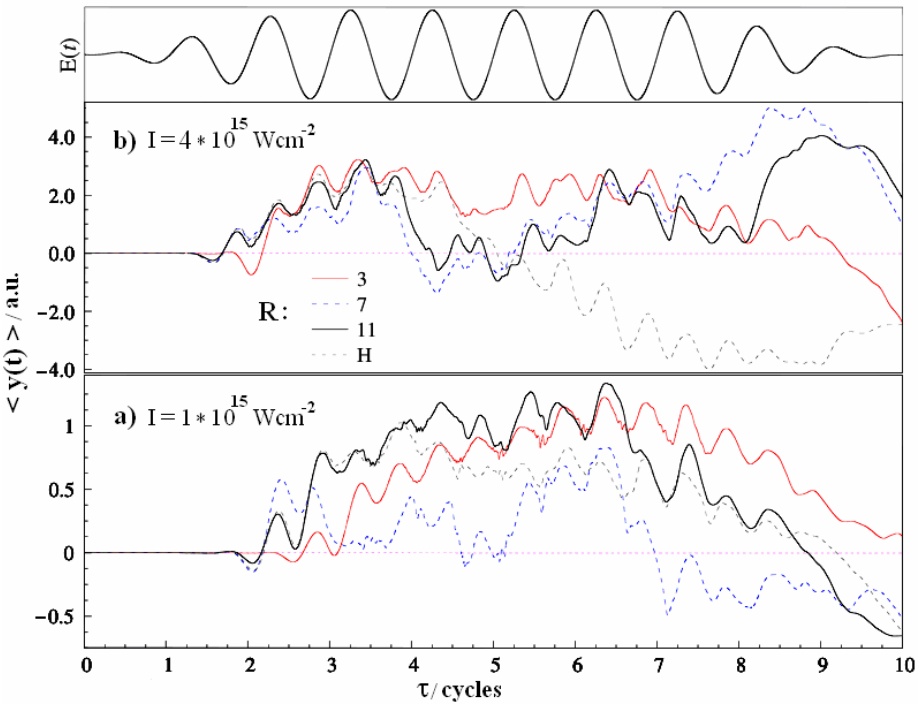

Fig. 6. Average value of electron displacement in the propagation direction for the *xy* 2-D H_2^+ molecular ion at R = 3.0, 7.0 and 11.0 *au* in its ground state under combined magnetic and electric field interactions in a 10-cycle (3,4,3) linearly polarized laser pulse with 0.057 frequency and $I = 1 \times 10^{15}$ Wcm^{-2} (a) and $I = 4 \times 10^{15}$ Wcm^{-2} (b) intensity. The results of the same calculations for the hydrogen atom are plotted (the dotted gray curve) for comparison. The horizontal axis is scaled in terms of the number of cycles of the laser pulse (depicted atop). The $< y(t) > = 0$ (horizontal) line in each panel corresponds to the calculations in the absence of magnetic field interaction, *i.e.*, the case (ii) Hamiltonian including only the electric field interaction.

wavelength (λ = 800 nm), but with shorter pulse length (with a 3-4-3 cycle sequence) at two different intensities (I = 1.0 × 10^{15} Wcm^{-2} and I = 4.0 × 10^{15} Wcm^{-2}). To avoid the fast depletion of the WP at these high intensities [26], the box size was increased to 400 × 200 *au* (in the polarization and propagation directions, *x* and *y*, respectively) but with the same grid and NIP setup.

Figure 6 shows an oscillating drift with a complex pattern in the electron WP displacement along the propagation direction due to the magnetic component of the Lorentz force of the laser pulse. The fluctuating amplitude of the drift is distinct even for this long-wavelength laser pulse, and increased with increasing intensity of the laser pulse. Observation of the perpendicular drift prior to considerable ionization of the WP is in agreement with the results reported by Førre *et al.* [15] and Fischer *et al.* [16]. Analysis of the time-dependent norm of the H_2^+ electron WP under the laser field with the two I = 1.0 × 10^{15} Wcm^{-2} and I = 4.0 × 10^{15} W cm^{-2} intensities (not presented here for brevity) shows that at higher inter-nuclear distances, a major part of the WP is ionized during the first 5 cycles of the laser pulse within which the drift of the electron WP is in the positive direction. From Fig. 6, it can be seen clearly that the drift and the pattern of the wiggling of the electron WP depend on the inter-nuclear distance R (thus on the binding potential of electron to the nuclei) and the laser pulse intensity I (thus the time evolution and velocity of the WP). Analysis of the results obtained at these two intensities shows evidently the charge resonance enhanced ionization at critical inter-nuclear distance around 7 *au*. Furthermore, the amplitude of the induced alternative angular momentum is increased with the intensity of the laser pulse.

Based on the results presented so far, it can be concluded that the pure magnetic effect appears as the rotational evolution of the WP in the *xy* plane. The combination effects of the electric and magnetic fields, in addition to the evolution in the polarization direction, produce a wiggling in the electron WP in the propagation direction. Dynamics of the electron WP in intense laser fields is thus determined by both electric and magnetic fields of the laser pulse and quantum spreading. By ignoring the magnetic interaction, dynamics of the WP is determined only by the electric field of the laser pulse along the polarization direction and thus spreading of WP along the propagation direction is inherently quantum mechanical. While, when the magnetic interaction is included, in addition to the changes in the trajectory of the WP along the polarization direction, the WP is also evolved along the propagation direction.

A corresponding pair of snapshots of the filmed time variations of the local fluxes on the boundaries during the WP evolution calculated for a laser pulse of I = 4.0 × 10^{14} Wcm^{-2}, λ = 800 nm and (4,10,4) cycles envelope scheme (Eq. (4)) with and without the magnetic interaction terms, *i.e.* cases (*i*) and (*ii*) Hamiltonians, are shown in Figs. 7a and b, respectively (the movies can be obtained from the journal site or from the authors). Comparison of these two snapshots (movies) and their corresponding flux map variations, especially the amplitudes of the blue and red $j(y)$ peaks, shows that symmetry of the local fluxes at the extremes of the polarization axis (borders of the simulation box) is broken due to the changes in the evolution of the WP induced by the magnetic field of the laser pulse. This behavior can be deduced in a different way by probing the differential flux at the borders in the propagation direction of the laser pulse (along the *y*-axis), defined as $\Delta j(y) = j(+y) - j(-y)$, under the two Hamiltonian cases (*i*) and (*ii*); The $\Delta j(y)$ values are calculated for the two cases of Hamiltonians when the H_2^+ (R = 9.0 *au*) electron WP is exposed to the same laser field. The results of these calculations, presented in Fig. 8, show that in the absence of the magnetic interaction, *i.e.* case (*ii*), the fluxes in the $+y$ and $-y$ directions are equal and thus $\Delta j(y)$ is zero. By introducing the magnetic interaction to the Hamiltonian, *i.e.* case (*i*), the fluxes in the $+y$ and $-y$ directions remain no longer equal and thus $\Delta j(y)$ deviates from zero. Therefore, non-zero differential flux in the propagation direction of the laser pulse is a consequence of the magnetic field effect of the laser pulse. This clearly suggests that an angle-resolved electron spectroscopy can successfully probe the contribution of the magnetic interaction to the spatio-temporal evolution of the WP under intense laser fields.

Comparison of the WP evolution with and without the magnetic interaction, can be expressed in terms of the instantaneous differential norm of the WP defined as $\Delta|\psi(x,y)|^2 = |\psi_{B,E}(x,y)|^2 - |\psi_E(x,y)|^2$, or simply $\Delta n = n_{E,B}(x,y) - n_E(x,y)$, calculated for all grid points of the simulation box. A snapshot of the filmed time evolution of the differential norm

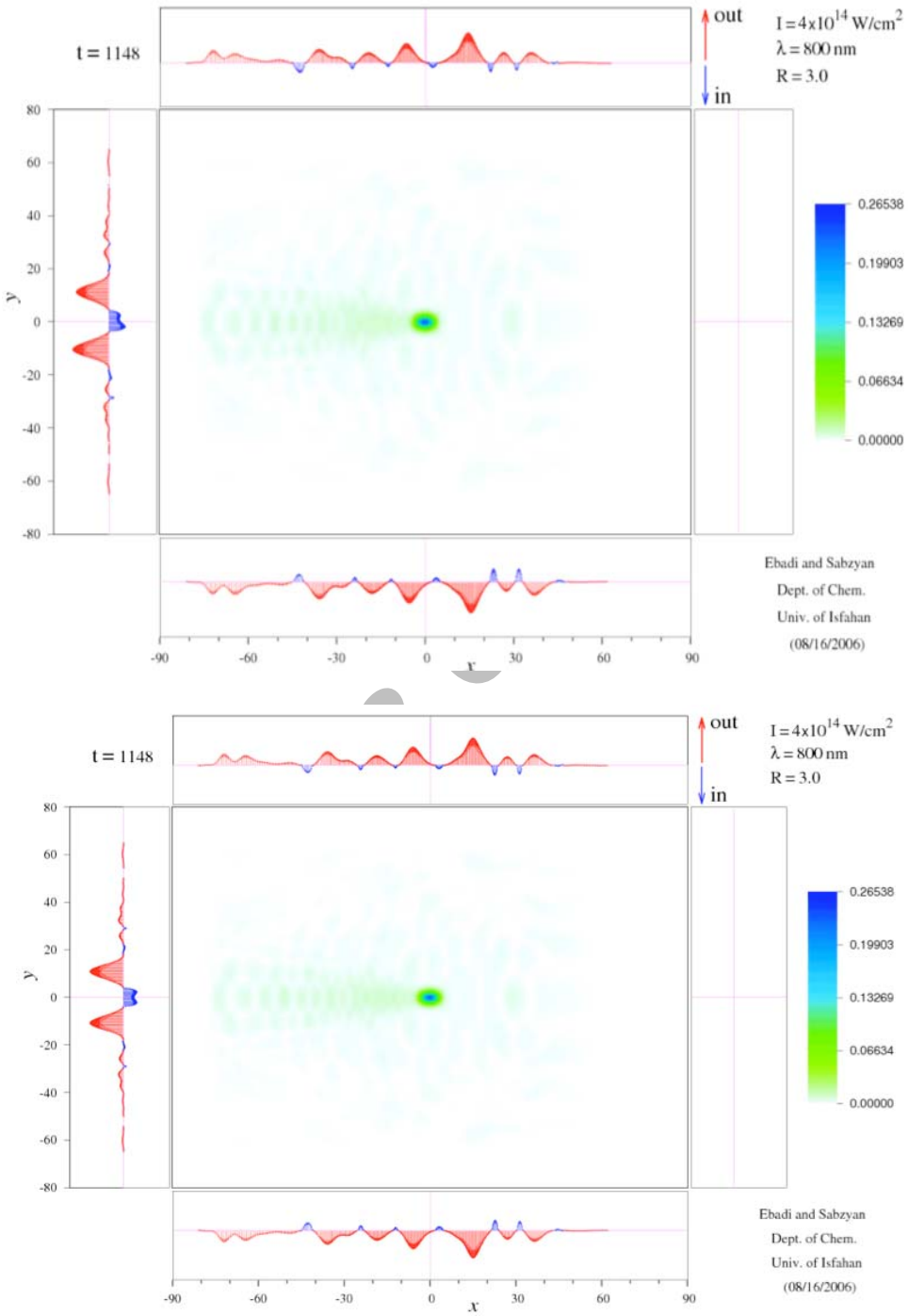

Fig. 7. Snapshot (at t = 1148 *au*) of the evolution of the electron WP norm and its fluxes at the boundaries of the simulation box for the *xy* 2-D H_2^+ molecular ion ($R = 3.0\,au$) in its ground state under the combined magnetic and electric field interactions with the case (*i*) Hamiltonian (top), and the pure electric interaction with the case (*ii*) Hamiltonian (bottom) in an 18-cycle (4,10,4) laser pulse of $I = 4.0 \times 10^{14}$ Wcm^{-2}, $\lambda = 800$ nm ($\omega = 0.0561$, $E_0 = 0.1067$). The instantaneous color scale of the norm is shown on the left. The input (*in*) and output (*out*) fluxes are shown in blue and red, and the scales of the $j(x)$and $j(y)$ fluxes are 10^{-5} and 10^{-6}, respectively. Note the asymmetric $j(y)$ flux in (a) as compared to the corresponding symmetric $j(y)$ in (b). The corresponding animations can be obtained from the authors.

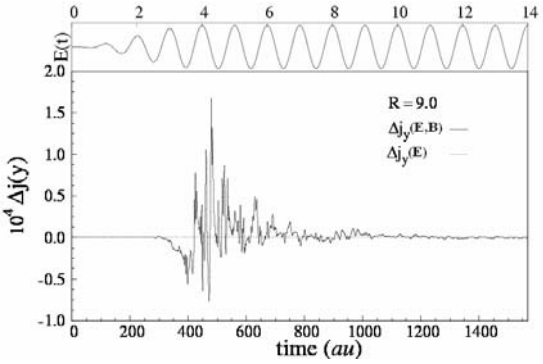

Fig. 8. The time variation of the differential flux in the propagation direction (y), $\Delta j(y) = j(+y) - j(-y)$, during the evolution of the WP of the xy 2-D model of H_2^+ at $R = 9.0$ *au* obtained under the influence of a (4,10,4) cycles laser pulse of $I = 4.0 \times 10^{14}$ Wcm^{-2} intensity and $\lambda = 800$ nm wavelength with and without the magnetic interaction; denoted by (E,B) and (E), respectively. The relevant part of the pulse scheme is plotted atop of the diagram.

Δn calculated for H_2^+ (R = 12.0 *au*) electron WP exposed to the laser pulse of $I = 4.0 \times 10^{14}$ Wcm^{-2}, and $\lambda = 800$ nm with a 4-10-4 cycles envelope, is shown in Fig. 9 (the movie can be obtained from the journal site or from the authors). Non-zero values of the differential WP at different grid points shown in this figure are evidences for the changes in the trajectory of the WP induced by magnetic interaction. The electric field interaction is significantly dominant at this intensity of the laser pulse; therefore, the evolved WP undergoes fast ionization and does not last (inside the simulation box) long enough to undergo spiral evolution under the significantly weaker magnetic field.

To visualize the magnetic field effect on the evolution of the WP more closely, interaction of the H_2^+ electron WP initially in the 4th excited state (n = 5, $^2\Pi$), at inter-nuclear separation R = 12.0 *au* with the magnetic field, *i.e.* case (*iii*) Hamiltonian, of a laser pulse of $I = 4.0 \times 10^{18}$ Wcm^{-2}, intensity, $\lambda = 800$ nm wavelength and a 4-10-4 cycles

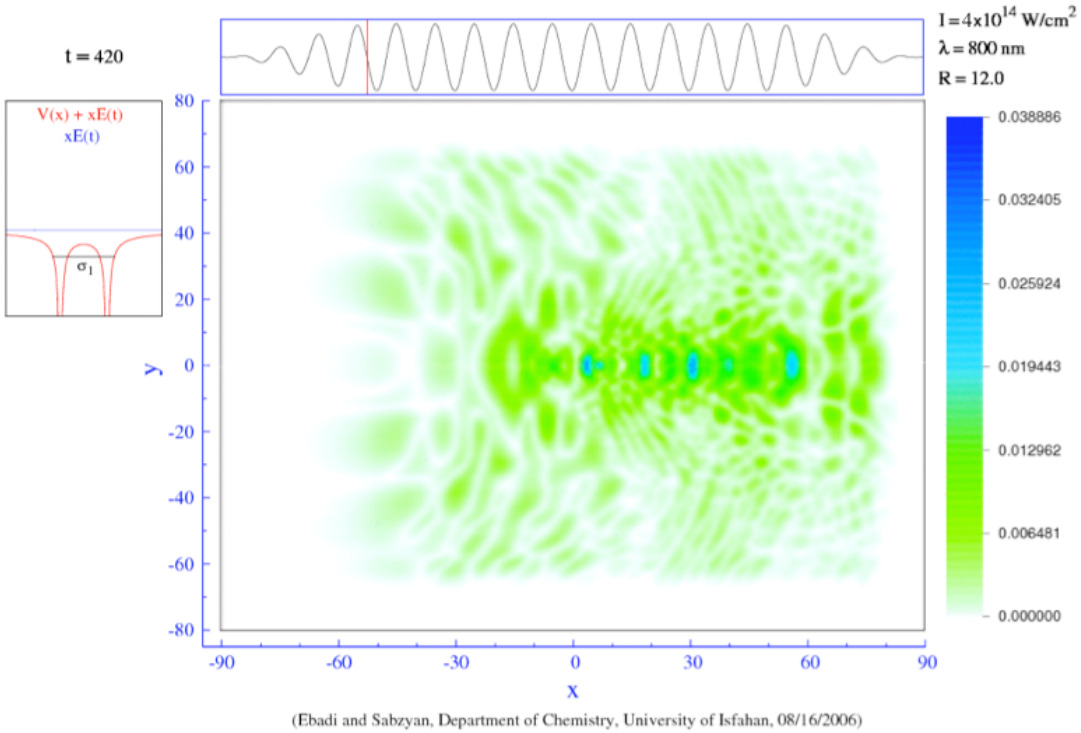

Fig. 9. A snapshot of the animation of the time-dependent differential electron WP norm, $\Delta n = n_{E,B}(x,y) - n_E(x,y)$, of the xy 2-D H_2^+ molecular ion at R = 12.0 *au* initially in its ground state in an 18-cycle (4,10,4) linearly polarized laser pulse with $\omega = 0.0561$, $E_0 = 0.1067$ ($I = 4.0 \times 10^{14}$ Wcm^{-2}, $\lambda =$ 800 nm). The pulse scheme and the corresponding time of the snapshot (the red vertical line segment) are shown atop. The corresponding animation can be obtained from the authors.

envelope is simulated. The n = 5, $^2\Pi$ state is the first electronic state of the *xy* 2-D model of H_2^+ with non-zero angular momentum and thus can interact immediately with the magnetic field of the laser pulse. The results of this simulation are filmed in a movie one of whose snapshots is shown in Fig. 10 (the movie is accessible from the journal site or can be obtained from the authors). As can be viewed from this movie, the WP including its segments is evolved in the *xy* plane around the *z*-axis under the influence of the magnetic interaction. Over the first few cycles of the laser pulse, the induced angular momentum and rotation of the WP are small but at longer times, the excess induced angular momentum causes more rotation of the WP during the evolution. Because of zero angular momentum, the ground state of H_2^+, as the starting WP, is not affected by the case (*iii*) Hamiltonian (only magnetic field), and thus simulation does not exhibit any change in the shape of WP. The laser intensity of I = 4.0 × 10^{18} Wcm^{-2} falls in the relativistic regime if the electric field interaction is included in the Hamiltonian [27,28]. Application of both electric and magnetic terms at this intensity would result in the explosion of the electron WP and induce electron velocities comparable to the velocity of light, and thus basically cannot be handled with the model used in the present article. We used this ultra high intensity to clearly visualize the pure contribution of the magnetic field term of the interaction Hamiltonian to the spatial evolution of the electron WP.

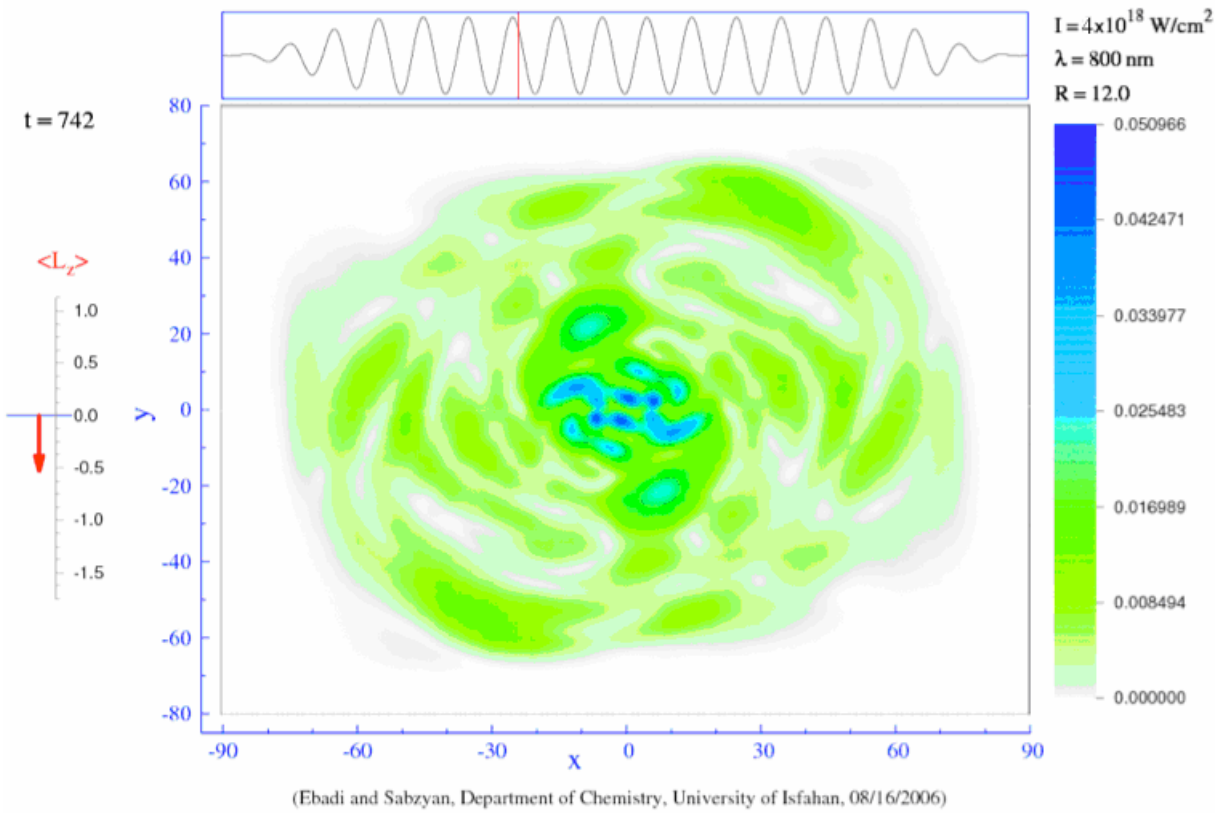

Fig. 10. A snapshot (at t = 742 *au*) of the *xy* 2-D H_2^+ (R = 12.0 *au*) electron WP evolution starting from the 4th excited state under the pure magnetic interaction in an 18-cycle (4,10,4) linearly polarized laser pulse with $\omega = 0.0561$ and $E_0 = 10.67$ (I = 4.0 × 10^{18} Wcm^{-2}, λ = 800 nm). Variation of the induced angular momentum and the instantaneous scale of the color map are shown on the left and right, respectively. The pulse scheme and the corresponding time of the snapshot (the red vertical line) are shown atop. The corresponding animation movie can be obtained from the journal site or from the authors.

CONCLUSIONS

The ionization rates and the decay pattern of the exponential norm of the *xy* 2-D model of H_2^+ are dominantly determined by the electric field of the laser pulse. Effect of the magnetic field of the laser pulse on the ionization rate appears as a phase shift and time delay of the norm decay, which are different in different inter-nuclear distances. The maximum phase shift of the ionization rate is about 7 *au* equivalent to 0.0625 cycle of the laser pulses of intensities in the tunneling regime. This effect is a consequence of the magnetic interaction which results in the changes in the trajectory of the electron wavepacket (WP) and the ionization channel. In the 2-D model of H_2^+, the generated *z*-component angular momentum interacts with the magnetic field of the laser pulse and consequently induces larger angular momentum compared with the case in which the magnetic field effect is absent. The pure magnetic effect appears as a spiral evolution of the WP in the *xy* plane. The combination effects of the electric and magnetic fields of the laser pulse results in the wiggling of the electron WP in the propagation direction. Amplitude and extent of this wiggling and its pattern depends strongly on the inter-nuclear distance and laser parameters.

The picture of the time evolution of the local flux densities on the boundaries during the evolution of the WP under the combined magnetic and electric fields interactions show that the symmetry of the local fluxes at the borders along the polarization axis is broken due to the significant changes in the evolution of the WP induced by the magnetic field of the laser pulse.

Although inclusion of the magnetic field interaction term in the Hamiltonian may not significantly affect the net ionization rate, it certainly changes the angle-resolved ionization rates as well as the spatial fragmentation pattern which can then be detected by appropriate experimental setup. The extents of the magnetic field interaction for different *xy* contours (slices) of the electron WP of the H_2^+ system along the *z*-axis in the actual 3-D model are different. Therefore, it can be expected that the presence of the magnetic field in the interaction Hamiltonian of the 3-D H_2^+ in intense laser fields, besides the induced evolutions along the *x* and *y* axes derived in this 2-D study, would also result in an extra evolution of the WP along the *z*-axis, in addition to the evolution induced by the electric field of the laser pulse.

A comrehensive picture of the magnetic field effect on the evolution of the 3-D H_2^+ electron WP under intense laser fields can be obtained by solving the relativistic TDSE in the coulomb gauge without dipole approximation.

ACKNOWLEDGMENTS

We gratefully acknowledge supports of the research and graduate offices of the University of Isfahan.

REFERENCES

[1] M. Protopapas, C.H. Keitel, P.L. Knight, Rep. Prog. Phys. 60 (1997) 389.
[2] A.T. Le, X.M. Tong, C.D. Lin, Phys. Rev. A 73 (2006) 041402(R).
[3] A. Scrinzi, M.Y. Ivanov, R. Kienberger, D.M. Villeneuve, J. Phys. B: At. Mol. Opt. Phys. 39 (2006) R1.
[4] K. Harumiya, H. Kono, Y. Fujimura, I. Kawata, A.D. Bandrauk, Phys. Rev. A 66 (2002) 043403.
[5] T. Kato, H. Kono, Chem. Phys. Lett. 392 (2004) 533.
[6] Y. Sato, H. Kono, S. Koseki, Y. Fujimura, J. Am. Chem. Soc. 26 (2003) 8019.
[7] M. Vafaee, H. Sabzyan, J. Phys. B: At. Mol. Opt. Phys. 37 (2004) 4143.
[8] A.D. Bandrauk, H. Lu, J. Chem. Phys. 4 (2001) 115.
[9] A.D. Bandraukand, H. Shen, J. Chem. Phys. 99 (1993) 1185.
[10] J.R. Vázques de Aldana, L. Roso, Opt. Express 5 (1999) 144.
[11] M.Y. Ryabikin, A.M. Sergeev, Optics Express 12 (2000) 417.
[12] M. Protopapas, C.H. Keitel, P.L. Knight, J. Phys. B: At. Mol. Opt. Phys. 29 (1996) 591.
[13] M.W. Walser, D.J. Urbach, K.Z. Hatsagortsyan, S.X. Hu, C.H. Keitel, Phys. Rev. A 65 (2002) 043410.
[14] C.H. Keitel, P.L. Knight, Phys. Rev. A 51 (1995) 1420.
[15] M. Førre, J.P. Hansen, L. Kochbach, S. Selstø, L.B. Madsen, Phys. Rev. Lett. 97 (2006) 043601.
[16] R. Fischer, M. Lein, C.H. Keitel, Phys. Rev. Lett. 97 (2006) 143901.
[17] B.R. Tembery, R. Taïeb, V. Véniard, A. Maquet, J. Phys. B: At. Mol. Opt. Phys. 35 (2002) 397.

[18] A.S. Alnaser, T. Osipov, E.P. Benis, A. Wech, B. Shan, C.L. Cocke, X.M. Tong, C.D. Lin, Phys. Rev. Lett. 91 (2003) 163002.
[19] A.V. Kim, M. Y. Ryabikin, A.M. Sergeev, Usp. Fiz. Nauk 58 (1999) 169.
[20] A.D. Bandrauk, H. Shen, Chem. Phys. Lett. 176 (1991) 428.
[21] G.D. Smith, Numerical Solution of Partial Differential Equations, Finite Difference Methods, 3rd ed., Oxford, Clarendon, 1986.
[22] H. Sabzyan, H. Ebadi, Iranian Journal of Science and Technology, In Press.
[23] L.-Y. Peng, D. Dundas, J.F. McCann, K.T. Taylor, I.D. Williams, J. Phys. B: At. Mol. Opt. Phys. 36 (2003) L295.
[24] A.D. Bandraukand, H.Z. Lu, J. Mol. Struct. 97 (2001) 547.
[25] M. Vafaee, H. Sabzyan, Z. Vafaee, A. Katanforoush, Phys. Rev. A 74 (2006) 054610.
[26] H. Sabzyan, M. Vafaee, Phys. Rev. A 71 (2005) 063404.
[27] A.D. Bandrauk, H.Z. Lu, Phys. Rev. A 73 (2006) 013412.
[28] M.W. Walser, C.H. Keitel, A. Scrinzi, T. Brabec, Phys. Rev. Lett. 85 (2000) 5082.